JOC The Journal of Organic Chemistry

Article

pubs.acs.org/joc

Panchromatic Sensitizer for Dye-Sensitized Solar Cells: Unsymmetrical Squaraine Dyes Incorporating Benzodithiophene π-Spacer with Alkyl Chains to Extend Conjugation, Control the Dye Assembly on TiO_2, and Retard Charge Recombination

Rajesh Bisht,[†,‡] Munavvar Fairoos M. K.,[†] Ambarish Kumar Singh,[†,‡] and Jayaraj Nithyanandhan*[,†,‡]

[†]Physical and Materials Chemistry Division, CSIR-National Chemical Laboratory, CSIR-Network of Institutes for Solar Energy, Dr. Homi Bhabha Road, Pune 411008, India

[‡]Academy of Scientific and Innovative Research (AcSIR), New Delhi 110025, India

Supporting Information

ABSTRACT: Metal-free near-infrared (NIR) active unsymmetrical squaraine dyes, **RSQ1** and **RSQ2**, with benzodithiophene (BDT) π-spacer and cyanoacrylic acid acceptor were synthesized by utilizing palladium catalyzed direct (hetero)arylation reaction. Methyl and 2-ethylhexyl groups were strategically placed at the BDT unit for **RSQ1** and **RSQ2**, respectively, to investigate the effect of alkylated π-spacer on dye aggregation on the TiO_2 surface and recombination reactions at TiO_2/dye/electrolyte interface. These dyes have strong absorption ($\varepsilon > 10^5$ M^{-1} cm^{-1}) in near-infrared (NIR) region and exhibit similar optical and electrochemical properties as they have same conjugated framework. **RSQ2** performed better than **RSQ1** owing to its higher open-circuit voltage (V_{oc}) and fill factor (ff) in spite of having comparable short-circuit current density (J_{sc}). The panchromatic incident photon-to-current conversion efficiency (IPCE) response was also observed for both the dyes. **RSQ2** showed power conversion efficiency (PCE) of 6.72% with short-circuit current density (J_{sc}) of 18.53 mA/cm^2, open circuit voltage (V_{oc}) of 0.538 V, and fill factor (ff) of 67.4%, without any coadsorbent. Attenuation of the charge recombination for **RSQ2** was revealed by electrochemical impedance analysis (EIS) and open-circuit potential decay transients (OCVD), which attributes to its higher V_{oc} and ff in comparison to **RSQ1**.

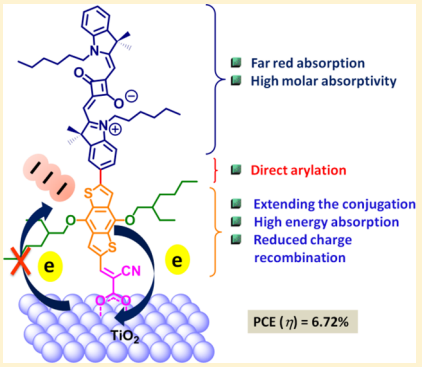

INTRODUCTION

Dye-sensitized solar cells (DSSCs) have emerged as a prominent photovoltaic technology where organic or organometallic sensitizers are used as light harvesting component for photon-to-current conversion.[1] Photosensitizers anchored to the mesoporous layer of TiO_2 absorb photons and inject electrons into the conduction band of TiO_2. After the photoinduced charge separation, oxidized dyes are regenerated by reducing agents present in the electrolyte.[2] Ruthenium(II) polypyridyl complexes have been highly studied since the beginning as sensitizer and PCE of 11.5% was achieved for dye CYC-B11 using I^-/I_3^- redox couple.[3] Highest efficiency of 13% for organometallic dyes were reported by Mathew et al.[4] for Zn (II)-porphyrin complex (SM-315) in the presence of Co(II/III) redox couple. Although these metal complexes showed broad spectral coverage and high efficiency, low molar extinction coefficient at higher wavelength, and difficulty in synthesis led the attention toward metal-free alternatives.

Organic dyes have flexibility in terms of structural design and tuning of the molecular orbital energy levels, and their feasibility in synthesis makes them low cost alternative to metalated dyes.[5] Among metal-free dyes, PCE of 10.1% was achieved for a tetrathienoacene based dye (TPA-TTART-A)[6] with I^-/I_3^- electrolyte and an N-annulated indoperylene (C275) based dye[7] produced the efficiency of 12.5% with Co(II/III) based electrolyte. These metal-free D−π−A dyes even though are efficient, their photo response in far-red and NIR region is limited. To utilize this region of spectrum, there are limited chromophores available, which includes porphyrins,[8−11] pthalocyanine[12,13] and polymethine.[14] Squaraine dyes are subclass of polymethine dyes, which owing to its low band gap and strong absorption ($\varepsilon > 10^5$ M^{-1} cm^{-1}) in the visible and NIR region, have found application in various areas like photovoltaic,[15−17] bioimaging,[18,19] ion sensing[20] and photodynamic therapy.[21,22] When these dyes are in conjugation with π-spacers[23,24] as in YR6, JD10 and DTS-CA (Figure 1), apart from their intramolecular charge transfer (ICT) transition at higher wavelength, π−π transition at lower wavelength region of the spectrum is also observed, which makes them attractive as possible panchromatic sensitizers to harvest visible and NIR photons.

The initial results of the squaraine based DSSCs were poor compared to organometallic dyes because of strong aggregation on metal oxide surface, which hampered the IPCE, leading to low PCEs in the absence of coadsorbents (like 3α,7α-

Received: November 4, 2016
Published: January 25, 2017

DOI: 10.1021/acs.joc.6b02670
J. Org. Chem. 2017, 82, 1920−1930

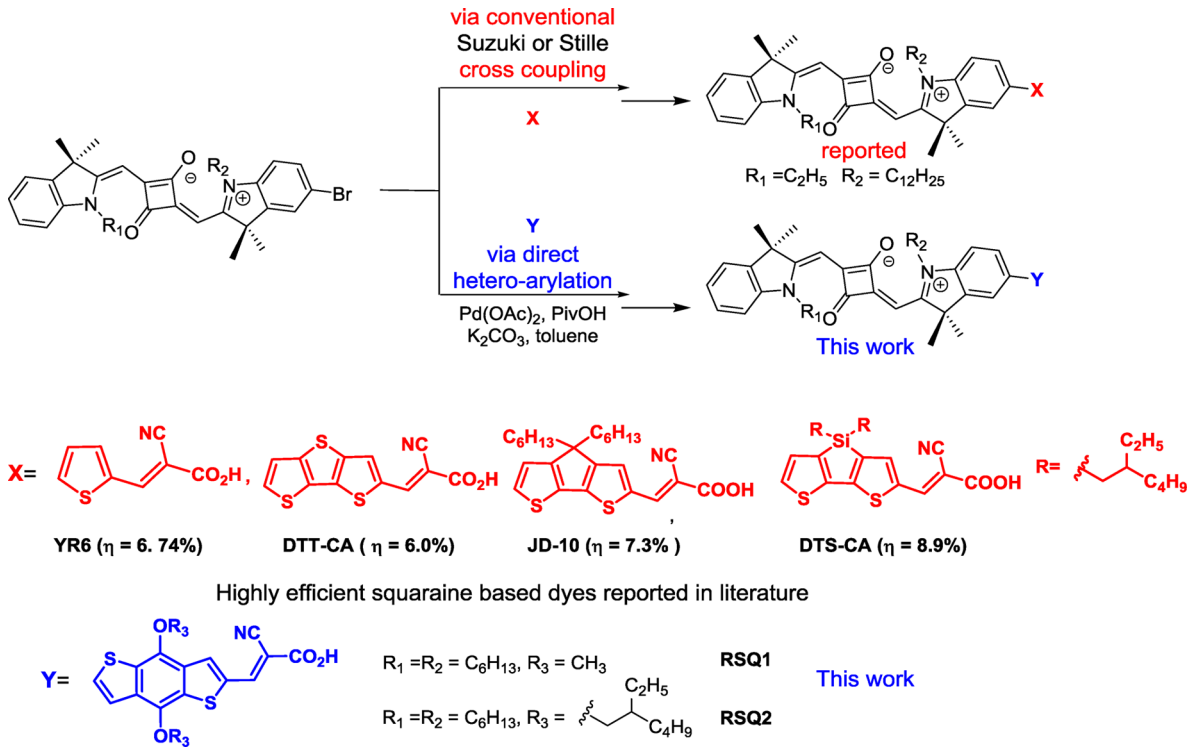

Figure 1. Reported squaraine dyes synthesized via conventional method and RSQ dyes synthesized via direct (hetero)arylation method for DSSCs.

dihydroxy-5β-cholanic acid, CDCA).[25−28] Aggregation of dyes on TiO_2 is common phenomenon and has variable effect on the performance of DSSCs.[25,26,29−31] These aggregates can be studied by UV−vis spectroscopy as blue-shifted (H-type aggregates) or red-shifted (J-type aggregates) absorption with respect to monomer absorption. In some cases aggregation helped in broadening the absorption spectra, which increased the light harvesting efficiency[29−31] whereas in many instances it reduced the photocurrent through self-quenching processes where significant portion of absorbed photons was wasted due to deactivation of the excited state.[25,26,32] Efforts have been made to increase the absorption of squaraine into the far-red region as well as to avoid aggregation by tuning the structural design. Yum et al.[33] reported the first unsymmetrical squaraine dye (SQ1) where carboxylic group was attached to the indolium group. The dye showed high molar extinction coefficient (ε_{max} = 1.58 × 10^5 M^{-1} cm^{-1}) corresponding to charge transfer (CT) transition, with λ_{max} at 636 nm and displayed a high IPCE response of 85% at 650 nm with an onset of 700 nm, which achieved an efficiency (η) of 4.5% with J_{sc} of 10.5 mA/cm^2 and V_{oc} of 0.603 V. The performance was further improved by replacing the indolium moiety by benzindolium moiety, which extended the conjugation further in far red region (λ_{max} = 662 nm) and improved molar absorptivity (ε_{max} = 3.19 × 10^5 M^{-1} cm^{-1}).[34] The dye exhibited maximum IPCE of 78%, J_{sc} of 11.3 mA/cm^2, V_{oc} of 0.667 V and hence improved PCE of 5.4% was achieved. Shi and co-workers[23] incorporated a thiophene bridge in indolium based squaraine dye (YR6) in attempt to enhance NIR absorption. The dye showed λ_{max} at 659 nm with a ε_{max} of 2.79 × 10^5 M^{-1} cm^{-1} and YR6-sensitized cell gave a J_{sc} of 14.8 mA/cm^2 and V_{oc} of 0.642 V, which led to an overall PCE of 6.74%. Delcamp and co-workers[24] experimented with various π-bridge and anchoring groups in squaraine dyes. Remarkably, JD-10 with cyclopentadithiophene (CPDT) bridge between squaraine and anchoring group exhibited absorption maximum at 680 nm and IPCE trace covering from 350 to 800 nm. In addition, the out-of-plane hexyl chains on CPDT helped to reduce dye aggregation, which produced PCE of 7.3%, with J_{sc} of 16.4 mA/cm^2 and V_{oc} of 0.635 V. Recently, Jradi et al.[35] reported a dye, DTS-CA, comparable to JD-10, in which they have 4-bis(2-ethylhexyl)-4*H*-silolo[3,2-b:4,5-b]dithiophene (DTS) linked covalently to a squaraine as a π-bridge. The two branched out-of-plane 2-ethylhexyl chains (on DTS) successfully avoided aggregation, which led to high photocurrent with IPCE onset at 850 nm with response of 90% at 700 nm and 82% at 500 nm. DSSC fabricated using the dye gave J_{sc} of 19.1 mA/cm^2 and V_{oc} of 0.682 V to yield an efficiency of 8.9%. Unsymmetrical squaraine dyes containing out-of-plane alkyl groups showed a superior device efficiency of 9.0% with the charge injection contribution from H-aggregates.[36] These results show that dye aggregation, light harvesting ability and charge transfer reactions at key interfaces can be modulated by having a suitable design, which can critically affect the performance of DSSC.

In this article, we report synthesis of squaraine dyes coupled with benzodithiophene (BDT) (**RSQ1** and **RSQ2**) to extend the conjugation for better light absorption toward longer wavelength. BDT was chosen to extend the conjugation as it has fused structure, which enhances conjugation and can be functionalized easily like thiophene. It is also fairly easy to synthesize in large scale and has been used extensively as a donor in Donor−Acceptor copolymers and small molecules for organic electronics and photovoltaics.[37,38] The use of BDT in DSSC is very limited and there are few reports available where BDT is used as π bridge in D−π−A type DSSC.[39−41] To understand the effect of alkyl chains on aggregation and device performance of these dyes, BDT with methyl and ethylhexyl group were judiciously used. BDT was connected to squaraine using palladium catalyzed direct heteroarylation instead of

DOI: 10.1021/acs.joc.6b02670
J. Org. Chem. 2017, 82, 1920−1930

Scheme 1. (a) Synthesis of Bromo-Functionalized Unsymmetrical Squaraine, 7; (b) Synthesis of RSQ1 and RSQ2 Dyes Involving Palladium Catalyzed Direct (Hetero)arylation

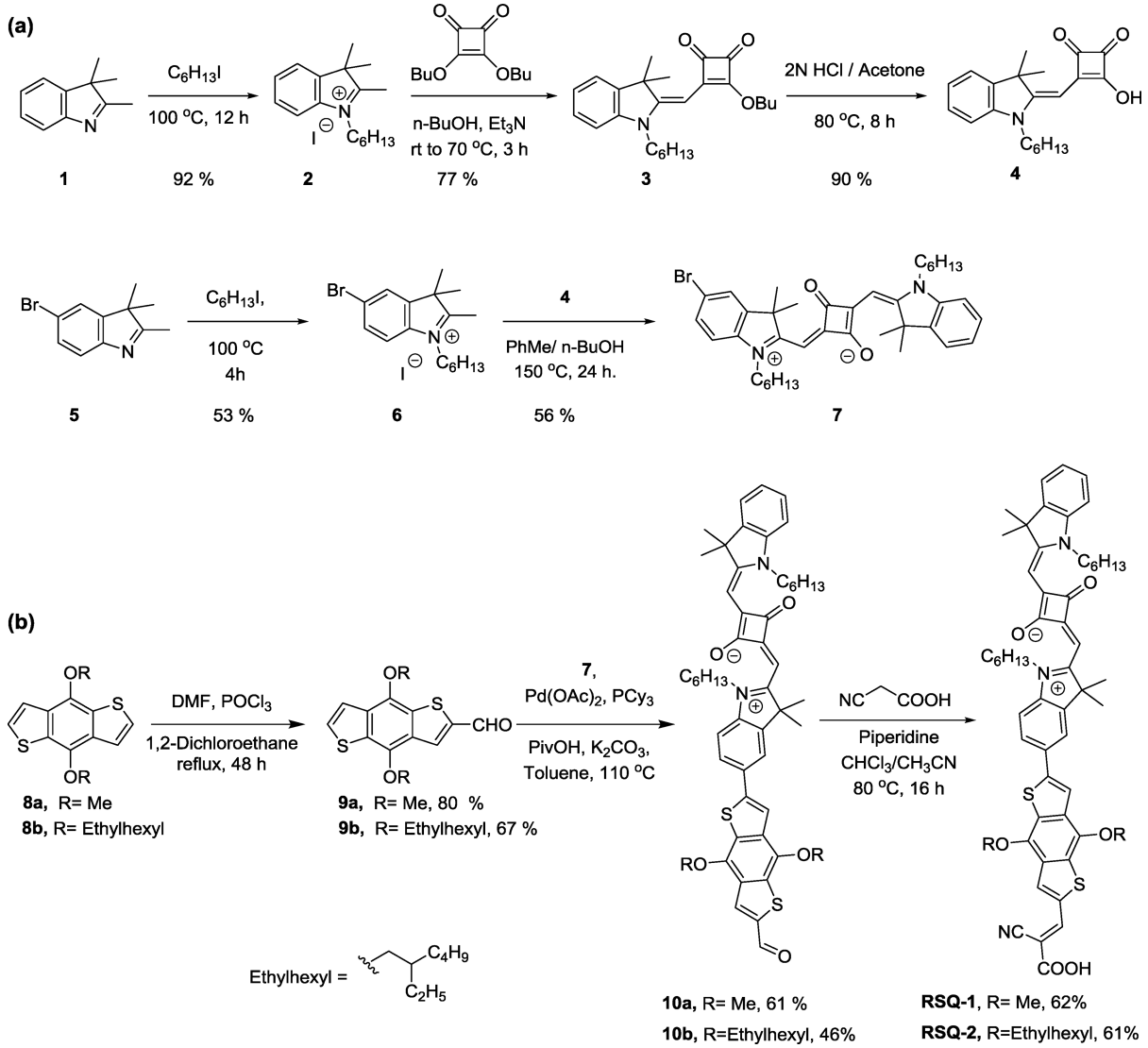

traditional C−C bond cross coupling like Suzuki, Negishi and Stille coupling. Though these traditional methods are efficient and consistent, they involve organometallic intermediates like boronic acids derivatives and organotin compounds, which makes them material exhaustive and time-consuming. Recently, direct arylation has emerged as a useful alternative to conventional cross-coupling where organometallic components are no longer required and simple arenes or heteroarenes can be used directly.[42−44] This method has been used to synthesize organic molecules for organic electronic and photovoltaic but its use in squaraine based molecules is rarely reported. We measured the photophysical properties of the dyes along with electrochemical properties. Current−voltage (I−V) characteristic with IPCE were also measured and compared for these dyes. **RSQ2** performed the best and achieved PCE of 6.72% with J_{sc} of 18.5 mA/cm^2, V_{oc} of 0.538 V, and fill factor of 67%, without any coadsorbent in the presence of I^-/I_3^- electrolyte.

RESULTS AND DISCUSSION

Synthetic approach to **RSQ1** and **RSQ2** is depicted in Scheme 1. The precursors, 5-bromo-2,3,3-trimethyl-3*H*-indole (**5**),[45] 4,8-dimethoxybenzo[1,2-b:4,5-b′]dithiophene[46] (**8a**) and 4,8-bis((2-ethylhexyl)oxy)benzo[1,2-b:4,5-b′]dithiophene[47] (**8b**) were synthesized according to the procedures known in the literature by Fischer Indole ring closing reaction of 4-bromophenylhydrazine, isopropylmethylketone and reductive alkylation of 4,8-dihydrobenzo[1,2-b:4,5-b′]dithiophen-4,8-dione with alkyl halide, respectively. Alkylation of 2,3,3-trimethyl-3*H*-indole (**1**) and, 5-bromo-2,3,3-trimethyl-3*H*-indole (**5**) was carried out with hexyl iodide to form the corresponding N-hexylated indolenine derivatives **2** and **6,** respectively. The indolium derivative **2** was treated with 3,4-dibutoxy-3-cyclobutene-1,2-dione to give semisquaraine, **3,** which was then hydrolyzed with 2 N HCl to give semisquaric acid **4**, quantitatively as a yellow color solid. The bromo-indolium derivative, **6** was condensed with the semisquaric acid **4** by azeotropic distillation of water employing Dean−Stark apparatus to afford bromo-functionalized unsymmerical squaraine dye **7** in moderate yield as a blue color solid. Aldehdye-functionalized BDT derivatives, **9a** and **9b,** were synthesized from their corresponding precursors **8a** and **8b** in good yields by Vilsmeier−Haack formylation reaction conditions of $POCl_3$,

DOI: 10.1021/acs.joc.6b02670
J. Org. Chem. 2017, 82, 1920−1930

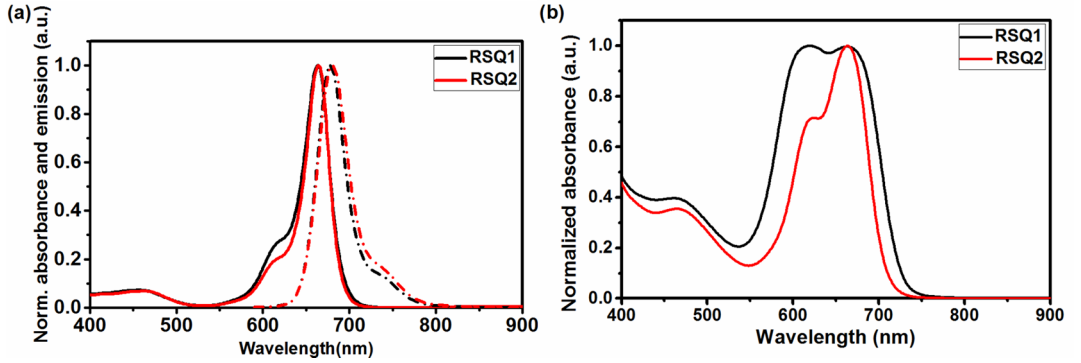

Figure 2. (a) Absorption (solid line) and emission (dotted line) spectra of **RSQ** dyes in $CHCl_3$ solution. (b) Normalized absorbance of RSQ dyes adsorbed at the surface of 6 μm thick TiO_2 film (Dye concentration = 0.1 mM in CH_2Cl_2, dipping time 30 min).

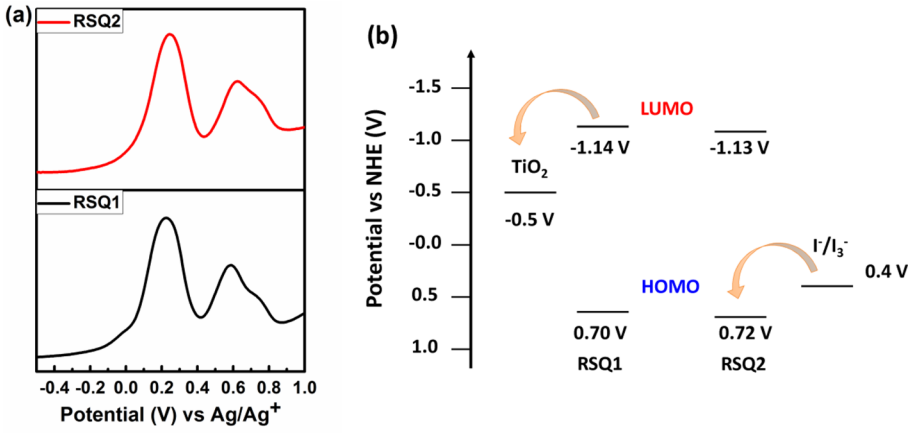

Figure 3. (a) Differential pulse voltammogram of RSQ dyes measured in CH_2Cl_2 (platinum wire as working electrode, nonaqueous Ag/Ag^+ (0.01M) as reference electrode and platinum foil as counter electrode) with $TBAClO_4$ (0.1 M) at the scan rate of 100 mV s^{-1}. (b) Energy level diagram for **RSQ1** and **RSQ2** with DSSC device components.

DMF in 1,2-dichloroethane for 48 h. The literature known methods generally involve lithiation of BDT derivative in strict moisture free environment and quenching with DMF but affords low reaction conversion.[39,48] We have optimized the Vilsmeier−Haack formylation conditions for the two **9a**, and **9b** derivatives, without strict anhydrous conditions. Bromo functionalized unsymmetrical squaraine derivative, **7** was coupled with **9a** and **9b** via $Pd(OAc)_2$ catalyzed direct arylation with Fagnou's protocol,[49] with PCy_3 as a coligand and pivalic acid as an additive in PhMe to provide the corresponding aldehyde precursors **10a**, and **10b** in moderate yield as green solid. Knoevenagel condensation of the aldehyde precursors **10a** and **10b** with cyanoacetic acid afforded the final compounds **RSQ1** and **RSQ2** respectively in moderate yields as green solid. The SQ-BDT dyes **RSQ1** and **RSQ2** are completely soluble in chlorinated solvents such as $CHCl_3$, CH_2Cl_2; **RSQ1** is soluble in ethanol and acetone, in which **RSQ2** is not soluble. All the synthesized compounds were duly characterized by NMR and mass spectrometry.

Photophysical Properties. The UV−vis absorption and emission spectra of **RSQ1** and **RSQ2** in $CHCl_3$ solution are shown in Figure 2a, and UV−vis spectra of **RSQ** dyes adsorbed on transparent mesoporous TiO_2 film is shown in Figure 2b.

The absorption spectra of both the dyes in solution exhibit intense absorption band in the range of 500 nm to700 nm. They have λ_{max} at 664 nm corresponding to intramolecular charge transfer (ICT) transition, with a high molar absorption coefficient (ε) of $2.18 \times 10^5$and 2.39×10^5 M^{-1} cm^{-1} for **RSQ1** and **RSQ2** respectively. There is a less intense band from 400 to 500 nm with extinction coefficient of 1.71×10^4 and 1.53×10^4 M^{-1} cm^{-1} at 455 nm, for **RSQ1** and **RSQ2** respectively. The presence of low intensity band had been observed previously, when the squaraine units were electronically extended with π-spacer.[24,35] Such spectral features help to absorb visible photons besides harvesting NIR photons. To understand the assembly of **RSQ1−2** dyes on TiO_2, the bare TiO_2 electrodes were dipped in to the CH_2Cl_2 solutions (0.1 mM) of the dyes and UV−vis spectra were recorded. The absorption spectra of dyes on TiO_2 film shows broadening of peaks due to aggregation. In addition to the monomeric peak at 663 nm, peaks at 619 nm for **RSQ1** and at 624 nm for **RSQ2** were observed. The emergence of peaks at shorter wavelength indicates formation of H-type aggregates on TiO_2 film, which is commonly known for squaraine based dyes.[34,50] In the case of **RSQ2** dye, the high energy aggregate peak was narrower and less prominent, suggesting the suppression of aggregation by branched alkyl chains. To gain the insight into the excited state nature of the dyes, the UV−vis absorption and fluorescence spectroscopy were carried out in different solvents. The spectra showed negative solvatochromism where λ_{max} shifts to shorter wavelength with increased polarity of solvents. This indicates that ground state is more polar than excited state in RSQ dyes. Such behavior has been reported previously in several squaraine dyes (Figure S24 and Table S5).[51,52] Fluorescence quantum yields were also calculated in different solvents and found to be

DOI: 10.1021/acs.joc.6b02670
J. Org. Chem. 2017, 82, 1920−1930

Table 1. Photophysical and Electrochemical Properties of RSQ Dyes

dyes	λ_{abs}/CH_2Cl_2 (nm)[a]	λ_{abs}/TiO_2 (nm)[b]	λ_{em} (nm)[a]	$\varepsilon \times 10^4$ (M^{-1} cm^{-1})[a]	$E_{g/DFT}$ (eV)	E_{ox} (V vs Ag/Ag^+)[c]	E_{HOMO} (V vs NHE)[c]	E_{0-0} (eV)[d]	E_{LUMO} (V vs NHE)[e]
RSQ1	455, 664	619, 663	678	1.71, 21.8	1.85	0.2258	0.70	1.84	−1.14
RSQ2	455, 664	624, 664	680	1.53, 23.9	1.85	0.2459	0.72	1.85	−1.13

[a]Absorption and emission spectra, molar extinction coefficients (ε) were measured in CH_2Cl_2. [b]6 μm transparent film was dipped in 0.1 mM of dye in CH_2Cl_2 for 30 min. [c]The oxidation potentials were measured in CH_2Cl_2 solutions with tetrabutylammonium perchlorate ($TBAClO_4$) as supporting electrolyte, ferrocene/ferrocenium (Fc/Fc^+) as an internal reference and converted to NHE by addition of 0.63 V. [d]Optical energy gaps (E_{0-0}) were deduced from the intersection of absorption and emission spectra, E_{0-0} (eV) = 1240/λ. [e]E_{LUMO} was calculated from E_{LUMO} (V vs NHE) = E_{HOMO} − E_{0-0}.

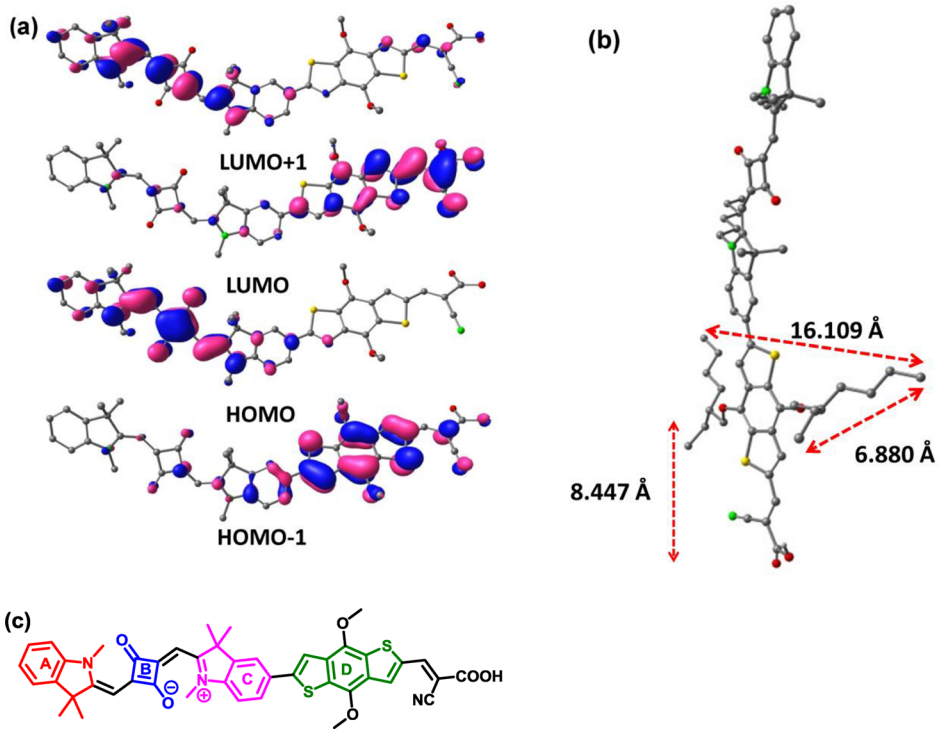

Figure 4. (a) Isodensity surface plots of HOMO−1, HOMO, LUMO and LUMO+1 of **RSQ** dyes (Hydrogen atoms and alkyl chains are removed for clarity). (b) DFT optimized structure of **RSQ2** (Distance between the terminal carbon atoms of hexyl units on BDT: 16.109 Å, distance between the terminal carbon atoms of ethylhexyl units on BDT: 6.880 Å, distance between the O atom (on BDT) of branching unit and O atom of carboxylic acid unit: 8.447 Å). (c) Dihedral planes shown as A, B, C and D on RSQ dye (alkyl chains are removed for clarification).

higher in the case of nonpolar solvent than in polar solvent like ethanol (Table S6).

Electrochemical Properties. In order to examine the feasibility of electron transfer at TiO_2/dye/electrolyte interfaces, ground state oxidation potential of the dye is compared with electrochemical potential of electrolyte (0.4 V vs NHE) and excited state potential of the dye is compared with the conduction band edge (−0.5 V vs NHE) of the TiO_2.[2,53] Redox potentials of **RSQ** dyes were measured by differential pulse voltammetry (DPV) (Figure 3a, 3b and Table 1) and cyclic voltammetry (Figure S25).

The first ground-state oxidation potential (E_{HOMO}) are found at 0.70 and 0.72 V vs NHE for **RSQ1** and **RSQ2** respectively, which are lower than electrochemical potential of I^-/I_3^- to ensure the dye regeneration. The excited state oxidation potential were calculated by subtracting E_{0-0} from E_{HOMO} and are found at −1.14 and −1.13 V for **RSQ1** and **RSQ2**, respectively. These values lie well above the conduction band edge of TiO_2, which predicts efficient charge injection into TiO_2. The optical band gap or ground state energy E_{0-0}, calculated from intersecting point of absorption and emission curve, were at 1.84 and 1.85 eV for **RSQ1** and **RSQ2** respectively, which are in good accordance to the band gaps calculated from the DFT studies.

Computational Studies. To predict the electronic distribution in RSQ sensitizer, geometry optimization was carried out using density functional theory (DFT) at B3LYP/6-31G(d,p) level with the Gaussian 09 program.[54] The electron density distributions for HOMO and LUMO are shown in Figure 4a.

For RSQ dyes, the electron distribution in HOMO is mainly located on squaraine part, whereas LUMO is located on BDT unit, which contains electron withdrawing cyanoacetic acid group. Such electron distribution in HOMO and LUMO suggests the effective electron transfer from donor to anchoring unit. The ethylhexyl chain around the RSQ2 stretches up to 16.1 Å along the plane of the molecule and 6.9 Å in out of plane direction, and the distance of bulky alkyl unit is about 8.4 Å from TiO_2 surface(Figure 4b). These structural features enhance the charge injection by reducing the dye aggregation by avoiding $\pi-\pi$ interaction and diminish the charge recombination by surface passivation due to hydrophobic

DOI: 10.1021/acs.joc.6b02670
J. Org. Chem. 2017, 82, 1920−1930

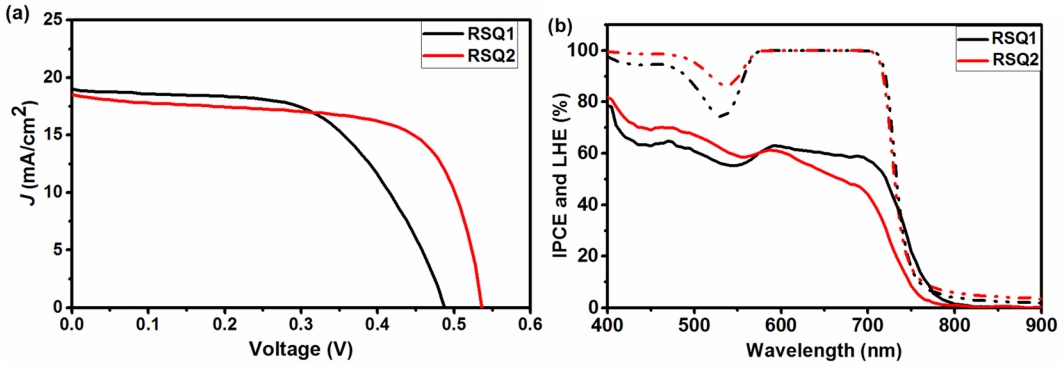

Figure 5. (a) $J-V$ curve and (b) IPCE spectrum (solid lines) and LHE spectrum (dotted lines) of RSQ sensitizers without coadsorbent. ([Dye] = 0.1 mM, in CH_2Cl_2, dipping time 5 h, TiO_2 active area = 0.22 cm^2).

alkyl chains near to TiO_2. Planarity of the dye has direct consequence on the degree of conjugation between donor and acceptor, which can be predicted from the dihedral angle between squaraine and BDT units of the dyes. Dihedral angles for the dyes were calculated from the optimized ground state geometry for the planes between indolenine units and squaric acid unit (A−B and B−C) and between BDT and SQ units (C−D) (Figure 4c). ∠**A−B** and ∠**B−C** shows that squaraine unit is almost planar in itself, whereas ∠**C−D** of 20.1° (**RSQ1**) and 25.5° (**RSQ2**) predicts that BDT is slightly out of plane, which shows slight restriction in the conjugation (Table S1).

Photovoltaic Properties. The photovoltaic performance of DSSC based on **RSQ1−2** dyes were evaluated under simulated AM 1.5 G illumination (100 mW cm^{-2}). The current density−voltage ($J-V$) characteristics of DSSCs are shown in Figure 5a and device performance data with and without coadsorbent are summarized in Table 2. **RSQ2** sensitized cells showed better performance in comparison to **RSQ1** without CDCA and achieved an overall power conversion efficiency (η) of 6.72% with a J_{sc} of 18.53 $mAcm^{-2}$, fill factor (ff) of 67.4% and V_{oc} of 0.538 V. **RSQ1** sensitized solar cells gave PCE of 5.43%, J_{sc} of 19.03 $mAcm^{-2}$, ff of 58.3% and V_{oc} of 0.490 V. The greater PCE of **RSQ2** is due to better V_{oc} and fill factor (ff) in comparison to **RSQ1**. Both enhancement in V_{oc} and ff in **RSQ2** could be attributed to controlled assembly of these dyes on TiO_2 surface.

Table 2. Photovoltaic Performance of RSQ Dyes with CDCA and without CDCA under 1 Sun Illumination

SQ dyes	V_{oc} (V)	J_{sc} (mA/cm^2)	ff (%)	η (%)[a]
RSQ1	0.490	19.03	58.3	5.43
RSQ1/CDCA (1 equiv)	0.488	18.25	59.4	5.29
RSQ1/CDCA (5 equiv)	0.494	15.08	58.6	4.36
RSQ1/CDCA (10 equiv)	0.495	9.47	58.5	2.74
RSQ2	0.538	18.53	67.4	6.72
RSQ2/CDCA (1 equiv)	0.539	18.77	67.7	6.84
RSQ2/CDCA (5 equiv)	0.545	15.53	68.8	5.82
RSQ2/CDCA (10 equiv)	0.539	14.14	68.5	5.22

[a]Photovoltaic performance of **RSQ** cells, thickness of electrode: 8 + 4 μm (transparent + scattering) layer of TiO_2, Electrolyte: 0.5 M DMII, 0.1 M LiI, 0.1 M I_2 and 10 mM TBP in CH_3CN. [Dye] = 0.1 mM in CH_2Cl_2, dipping time was 5 h, Active area of 0.22 cm^2 and measurements were carried out under 1 sun intensity (100 mW/cm^2).

To understand the aggregation effect, the dye was coadsorbed in the presence of (3α,7α-dihydroxy-5β-cholanic acid, (CDCA). Addition of CDCA generally helps in increasing the performance of DSSC by minimizing the aggregation, which can reduce the intermolecular self-quenching of excitons. Upon addition of 1 equiv of CDCA, the efficiency of the **RSQ2** dye improved to 6.84% with J_{sc} of 18.77 mA/cm^2 and V_{oc} of 0.539 V but for the **RSQ1** reduced to 5.29% with J_{sc} 18.25 mA/cm^2 and V_{oc} of 0.448 V. Here, difference in the PCE after addition of 1 equiv of CDCA appeared because of the small perturbation in the dye assembly. Further addition of CDCA decreases the device efficiencies as shown in the Table 2. PCE of **RSQ1** depleted to 4.36% when 5 equiv of CDCA was added due to decrease in short-circuit current density (J_{sc} = 15.08 mA/cm^2) and for **RSQ2**, PCE was decreased to 5.82% with J_{sc} of 15.53 mA/cm^2. PCE further decreased to 2.74% and 5.22% when 10 equiv of CDCA are added for **RSQ1** and **RSQ2**, respectively. This decrease in performance could be the result of reduced adsorption of the dye on the TiO_2 surface due to competitive adsorption of CDCA over dyes. To validate this hypothesis, dye desorption study was carried out to calculate the dye loading on TiO_2 films. The amount of dye loaded on TiO_2 for **RSQ1** and **RSQ2** sensitized DSSC was found to be 2.07×10^{-7} mol/cm^2 and 1.21×10^{-7} mol/cm^2 respectively. Even though the dye loading in **RSQ1** was almost twice the amount in **RSQ2**, hindered $\pi-\pi$ interaction and surface passivation by bulky alkyl group led to reduced charge recombination, which helped **RSQ2** based DSSC to attain better V_{oc} and ff. A drastic decrease in dye loading was observed for **RSQ1** (1.09×10^{-7} mol/cm^2) and **RSQ2** (0.67×10^{-7} mol/cm^2) when 10 equiv of CDCA was added. While the decrease in amount of dye load for both the dye was almost half to its initial values, the decrease in J_{sc} for **RSQ1** is much steeper (19.03 to 9.47 $mAcm^{-2}$) than for **RSQ2** (18.53 to 14.14 $mAcm^{-2}$). This observation could be attributed to the strong $\pi-\pi$ stack in **RSQ1** that does not allow the CDCA molecules to penetrate through them, whereas **RSQ2** was able to maintain the comparable J_{sc} by avoiding self-quenching of exciton due to weak $\pi-\pi$ interaction, which allows CDCA to break the aggregates efficiently.

IPCE and light harvesting efficiency (LHE) spectrum for DSSC based on **RSQ** dyes without coadsorbent is shown in Figure 5b. IPCE has direct consequence on short circuit current density (J_{sc}) of DSSC. **RSQ1** based DSSC has better IPCE response in the region of 600−800 nm, which corresponds to the absorption by monomers and aggregates. **RSQ2** compensates for this with greater IPCE between 400 and 560 nm, which corresponds to the absorption from π spacer. As a result **RSQ1** and **RSQ2** have comparable J_{sc} of 19.03 $mAcm^{-2}$ and

DOI: 10.1021/acs.joc.6b02670
J. Org. Chem. 2017, 82, 1920−1930

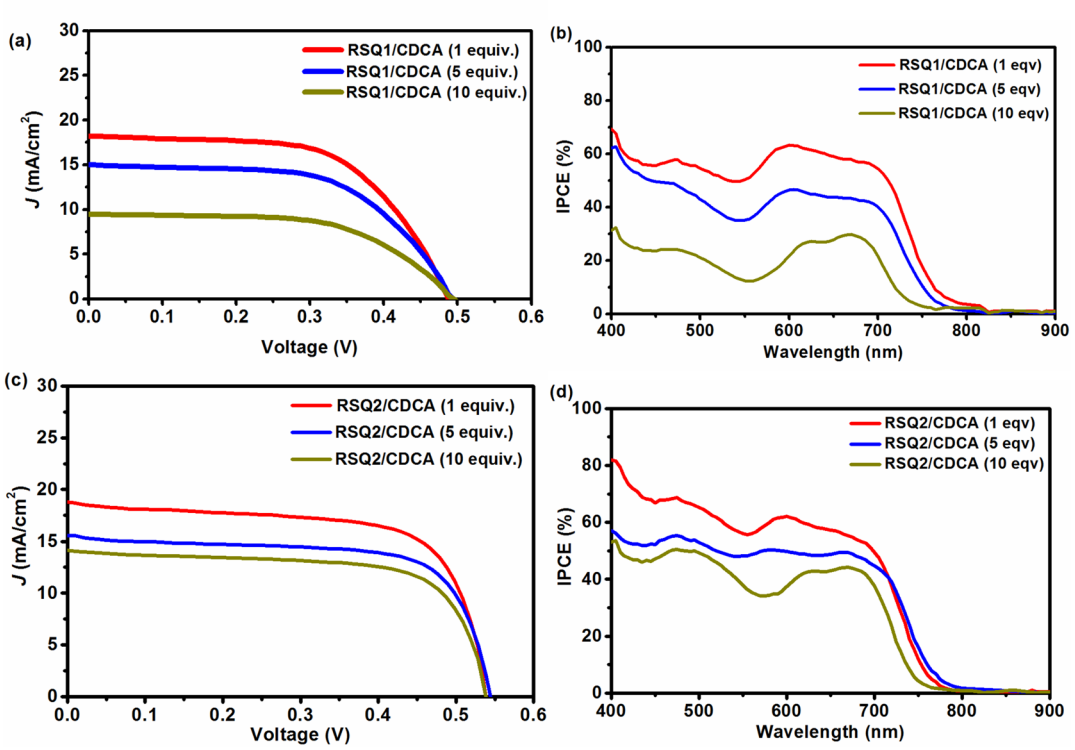

Figure 6. *J*–*V* curve and IPCE spectrum of RSQ sensitizers (solid lines) in the presence of CDCA.

18.53 mAcm^{-2} respectively. LHE (1-transmittance) shows the ability of sensitizers to absorb photons in the TiO_2 thin film. Both **RSQ** dyes showed more than 90% LHE from 400 to 750 nm except a small decrease around 540 nm. **RSQ2** shows better light harvesting efficiency in region of 400 to 550 nm in comparison to **RSQ1** but overlaps in the region 600–800 nm for both the dyes.

A gradual decrease in IPCE is observed with increasing concentration of CDCA, due to competitive binding of CDCA on TiO_2 (Figure 6b, 6d). When 5 equiv of CDCA were added, the IPCE dropped to 46% and 49% at 600 nm for **RSQ1** and **RSQ2** respectively. Addition of 10 equiv of CDCA further decreases IPCE due to reduction in dye content, which is particularly severe in case of **RSQ1**, as a result, IPCE is only 20% at 600 nm while it is 40% for **RSQ2**. Even though the effect of CDCA on deaggregation of dye could be observed from the IPCE trace, any expected improvement in IPCE is negated by the huge decrease in the amount of dye load.

Electrochemical Impedance Spectroscopy (EIS). In DSSC, changes in the Fermi level of electron in the TiO_2 and redox potential of electrolyte affect the V_{oc} and J_{sc}. The device sensitized with **RSQ1** and **RSQ2** exhibited comparable J_{sc}, of 19.03 mAcm^{-2} and 18.53 mAcm^{-2}, respectively. Hence, the increase in PCE of these two dyes could be ascribed to the distinct improvement in V_{oc} and *ff*. The factors that affect the V_{oc} and *ff* for a set of dyes, possessing similar conjugated framework, can be estimated by evaluating the electron transport resistance (R_{ct}) in the device across TiO_2/Dye/electrolyte interface and lifetime of injected electrons present in the conduction band of TiO_2 (E_{CB}). EIS analysis was carried out in the dark to understand the correlation between the charge transfer processes at the interfaces (TiO_2/dye/electrolyte) and the *ff* and V_{oc} without perturbing the self-assembled monolayer of dyes (Table 3). The Nyquist plots of the DSSCs based on the two RSQ dyes under an applied bias of −0.45 V in the dark with a frequency range of 1 Hz to 1 MHz are shown in Figure 7a.

Table 3. EIS Data for RSQ Dyes

SQ dyes	R_{ct} (ohm)	C_{μ} (mF)	*f* (Hz)	τ (ms)
RSQ1	9.53	0.775	25.06	6.35
RSQ2	12.73	0.833	17.74	8.97

The smaller semicircle at high frequency represents the impedance due to electron transfer at Pt/electrolyte interface, whereas the larger semicircle at midfrequency range corresponds to charge recombination resistance due to electron transfer from the TiO_2 film to the triiodide.[55,56] Larger the radius of the semicircle, larger is the resistance and hence smaller dark current. The radius of the larger semicircle for **RSQ2** (12.73 ohm) is greater than **RSQ1** (9.53 ohm), indicating greater electron recombination resistance at TiO_2/electrolyte interface, which is consistent with the enhanced V_{oc} and fill factor (*ff*). This could be due to slower electron recombination caused by bulky ethylhexyl group, which passivates the TiO_2 surface and reduced self-quenching of exciton by avoiding π–π stacking of dye molecules in **RSQ2** sensitized DSSC.

The electron lifetime is calculated from the peak frequency of the low-frequency peak in Bode phase plots Figure 7b. Electron lifetime is reciprocal of peak frequency and hence lower the peak frequency longer is the lifetime. Electron lifetime is higher for **RSQ2** (τ = 8.97 ms in comparison to **RSQ1** (τ = 6.35 ms), which further validates the higher V_{oc} and *ff* for **RSQ2**.

Open Circuit Voltage Decay Study (OCVD). Transient electron recombination kinetics of RSQ dyes based DSSCs were studied after illuminating the devices for 10 s under

DOI: 10.1021/acs.joc.6b02670
J. Org. Chem. 2017, 82, 1920–1930

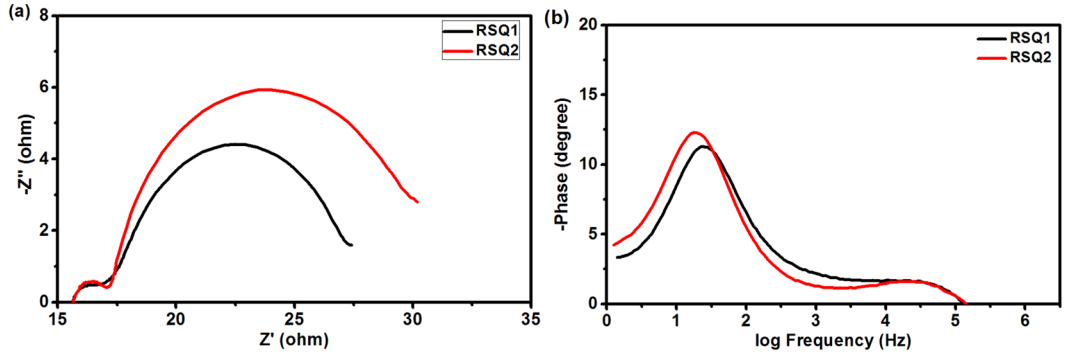

Figure 7. EIS data of RSQ dye cells. (a) Nyquist plot (applied bias of −0.45 V in the dark) and (b) Bode phase plot (electron lifetime is described as $\tau = 1/2\pi f$).

simulated sunlight (AM 1.5G, 100 mW/cm^2). Open-circuit voltage decay-time profile elucidates the electron recombination kinetics after in situ -generation of triiodide at proximity of sensitized photoanode/electrolyte interface via regeneration of oxidized dyes on TiO_2.

Decay profile of **RSQ2** (Figure 8) showed the slowest decay after turning off the light using a shutter, whereas the **RSQ1**

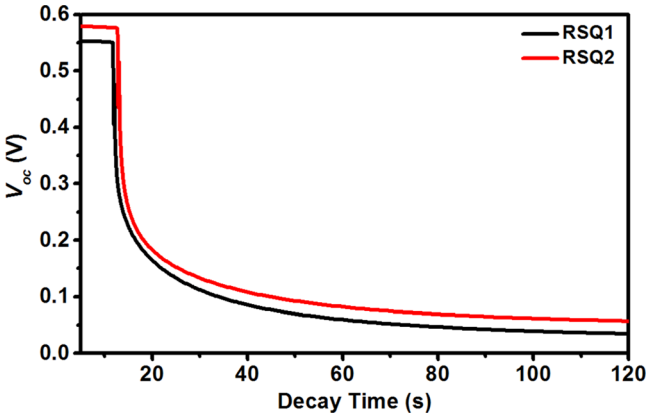

Figure 8. OCVD profiles of DSSCs based on **RSQ1**−**2** sensitizers and the experiments carried out under 1 sun intensity (100 mW/cm^2).

exhibited fastest decay. This further supports the strong ability of ethylhexylated BDT π-linker to attenuate the charge recombination process and increase the V_{oc} of **RSQ2**, which in turn resulted in the high PCE of 6.72%.

CONCLUSIONS

In order to exploit the far red and NIR region of solar spectrum for efficient DSSC, squaraine-benzodithiophene (SQ-BDT) based dyes, **RSQ1**, **RSQ2**, were synthesized. Squaraine were connected to BDT via direct arylation, which helps in reducing the number of synthetic steps. Both dyes exhibit good absorption in NIR region and have favorable energy levels for efficient charge transfer. UV−vis spectrum of dyes on thin TiO_2 films shows peak broadening for **RSQ1** as result of aggregation, whereas **RSQ2** has smaller aggregate courtesy of branched alkyl chains attached on BDT. DFT calculation predicts efficient electron transfer toward TiO_2 and also supports the photophysical and electrochemical observation. Owing to higher open circuit voltage (V_{oc}) and fill fator (*ff*), **RSQ2** sensitized DSSC gave the best photovoltaic performance with the PCE of 6.72%, without addition of any coadsorbents. Further, the addition of CDCA led to huge dip in dye loading on TiO_2 and proved to be detrimental to the device performance, which was more severe for the DSSC based on RSQ1. EIS analysis associates higher *ff* and V_{oc} of **RSQ2** with higher electron transfer resistance at TiO_2/electrolyte interface. This is mainly due to the reduced aggregation and surface passivation by branched alkyl chain in **RSQ2** based DSSC. The electron lifetime and OCVD supports V_{oc} trend and exhibits slower decay for **RSQ2** in comparison to **RSQ1**.

EXPERIMENTAL SECTION

General Methods. All reagents were purchased from commercial sources. Solvents were dried and distilled by standard procedures immediately before use. ^{1}H NMR and ^{13}C NMR were recorded in, $CDCl_3$, MeOH-d_4 or DMSO-d_6 on 200 MHz, 400 and 500 MHz NMR spectrometers. High-resolution mass spectrometric measurements were carried out using the ESI method and an ion-trap mass analyzer. Absorption spectra were recorded at room temperature in quartz cuvette using UV−visible spectrophotometer. The cyclic voltammetry (CV) and differential pulse voltammetry (DPV) analysis was carried out in anhydrous dichloromethane solvent by using 0.1 M tetrabutylammonium perchlorate as supporting electrolyte and Fc/Fc$^+$ as internal reference. The experiments were performed at room temperature in nitrogen atmosphere with a three-electrode cell consisting of a platinum foil as counter electrode, an Ag/Ag$^+$ reference electrode, and a platinum wire as working electrode.

Synthetic Procedure. *1-Hexyl-2,3,3-trimethyl-3H-indol-1-ium iodide (2).* A mixture of 2,3,3- trimethylindolenine **1** (2 g, 12.56 mmol) and *n*-hexyl iodide (3.2 g,15.07 mmol) was stirred and heated at 100 °C for 12 h. The reaction mixture was cooled to room temperature after the completion of reaction. The contents were dissolved in minimum amount of dichloromethane and poured over 100 mL of diethyl ether and filtered under vacuum. The precipitate obtained was washed with diethyl ether (20 mL × 3) to give pure compound **2** (4.3 g, 92%) as brown solid. mp 135−137 °C. ^{1}H NMR (200 MHz, $CDCl_3$) δ 7.71−7.49 (m, 4H), 4.76−4.54 (m, 2H), 3.10 (s, 3H), 2.04−1.82 (m, 2H), 1.64 (s, 6H), 1.51−1.18 (m, 6H), 0.86 (t, J = 6.9 Hz, 3H). ^{13}C NMR (101 MHz, MeOH-d_4) δ 197.6, 143.4, 142.5, 131.2, 130.5, 124.7, 116.6, 55.9, 49.5, 32.4, 28.9, 27.4, 23.5, 22.8, 14.3. HRMS (ESI) m/z [M]$^+$ Calcd for $C_{17}H_{26}N^+$ 244.2060, found 244.2053.

3-Butoxy-4-((1-hexyl-3,3-dimethylindolin-2-ylidene)methyl)-cyclobut-3-ene-1,2-dione (3). To solution of compound **2** (3.5 g, 9.43 mmol) in 25 mL of *n*-butanol, 3,4-dibutoxycyclobut-3-ene-1,2-dione (2.13 g, 9.43 mmol) was added. To the stirring mixture triethylamine (1.34 g, 13.2 mmol) was added dropwise. The resultant mixture was stirred at room temperature for 12 h followed by heating at 70 °C for 3 h. Solvents were evaporated after the completion of reaction and crude product was purified by column chromatography by silica gel to give compound **3** (2.9 g, 77%) as yellow solid. mp 85−87 °C. ^{1}H NMR (400 MHz, $CDCl_3$) δ 7.31−7.24 (m, 2H), 7.12−7.00 (m, 1H), 6.88

DOI: 10.1021/acs.joc.6b02670
J. Org. Chem. 2017, 82, 1920−1930

(dd, J = 7.1, 1.4 Hz, 1H), 5.41 (s, 1H), 4.86 (t, J = 6.6 Hz, 2H), 3.87−3.75 (m, 2H), 1.93−1.80 (m, 2H), 1.74 (d, J = 7.4 Hz, 2H), 1.63 (d, J = 4.5 Hz, 6H), 1.52 (dd, J = 15.0, 7.5 Hz, 2H), 1.46−1.38 (m, 2H), 1.35 (ddd, J = 7.3, 4.5, 2.5 Hz, 4H), 1.01 (t, J = 7.4 Hz, 3H), 0.90 (t, J = 7.1 Hz, 3H). ^{13}C NMR (101 MHz, $CDCl_3$) δ 192.8, 187.7, 187.6, 173.7, 168.5, 142.8, 141.0, 127.8, 122.8, 122.1, 108.5, 81.4, 73.9, 48.1, 43.1, 32.3, 31.5, 27.1, 26.8, 26.4, 22.60, 18.9, 14.1, 13.8. HRMS (ESI) m/z $[M + H]^+$ Calcd for $C_{25}H_{34}NO_3$ 396.2539, found 396.2530.

*3-((1-Hexyl-3,3-dimethylindolin-2-ylidene)methyl)-4-hydroxycyclobut-3-ene-1,2-dione (**4**).* To a solution of compound **3** (2.45 g, 6.194 mmol) in 15 mL of acetone, 5 mL of 2 N HCl was added. Resultant mixture was refluxed for 8 h, and solvents were removed under reduced pressure after the completion of reaction. The crude compound **1c** (1.98 g, 94%), obtained as dark yellow solid, was used further without purification. mp 170−172 °C. ^{1}H NMR (400 MHz, $CDCl_3$) δ 10.01 (s, 1H), 7.31 (dd, J = 10.2, 7.9 Hz, 2H), 7.13 (t, J = 7.4 Hz, 1H), 6.96 (d, J = 7.8 Hz, 1H), 5.68 (s, 1H), 3.91 (t, J = 6.6 Hz, 2H), 1.82−1.74 (m, 2H), 1.67 (s, 6H), 1.43 (d, J = 6.1 Hz, 2H), 1.39−1.31 (m, 4H), 0.90 (t, J = 6.8 Hz, 3H). ^{13}C NMR (101 MHz, $CDCl_3$) δ 189.9, 187.6, 176.9, 170.7, 142.5, 141.4, 128.0, 123.6, 122.2, 109.2, 82.4, 48.7, 43.5, 31.5, 29.8, 27.0, 26.7, 26.6, 22.6, 14.0. HRMS (ESI) m/z $[M + H]^+$ Calcd for $C_{21}H_{25}NO_3$ 340.1913, found 340.1903.

*5-Bromo-1-hexyl-2,3,3-trimethyl-3H-indol-1-ium iodide (**6**).* A mixture of 5-bromo-2,3,3-trimethyl-3*H*-indole **5** (1.7 g, 7.14 mmol) and *n*-hexyl iodide (1.82 g, 8.56 mmol) was heated at 100 °C for 4 h. Reaction mixture was cooled to room temperature after the completion of the reaction. The contents were dissolved in minimum amount of dichloromethane and precipitated by pouring in 100 mL of diethyl ether. The precipitate obtained was washed with diethyl ether (20 mL × 3) and dried under vacuum to give compound **6** (1.7 g, 53%) as dark brown solid. mp 208−210 °C. ^{1}H NMR (200 MHz, DMSO-d_6) δ 8.20 (s, 1H), 7.96 (d, J = 8.5 Hz, 1H), 7.85 (d, J = 8.7 Hz, 1H), 4.43 (t, J = 7.4 Hz, 2H), 2.84 (s, 3H), 1.80 (s, 2H), 1.55 (s, 6H), 1.30 (s, 6H), 0.86 (s, 3H). ^{13}C NMR (101 MHz, $CDCl_3$) δ 198.1, 145.5, 141.7, 133.7, 128.3, 128.2, 125.3, 118.3, 56.1, 49.8, 32.4, 28.8, 27.4, 23.5, 22.7, 14.3. HRMS (ESI) m/z $[M]^+$ Calcd for $C_{17}H_{25}BrN^+$ 322.1165, found 322.1160.

*4-((5-Bromo-1-hexyl-3,3-dimethyl-3H-indol-1-ium-2-yl)methylene)-2-((1-hexyl-3,3-dimethylindolin-2-ylidene)methyl)-3-oxocyclobut-1-en-1-olate (**7**).* A mixture of compound **6** (0.3 g, 0.88 mmol) and compound **4** (0.478 g, 1.06 mmol) in 16 mL of toluene/*n*-butanol (1:1) was refluxed under dean-stark apparatus for 24 h. After the completion of reaction the solvents were removed under reduced pressure and crude product was purified by column chromatography by silica gel using ethyl acetate/dichloromethane as eluent to yield compound **7** (0.32 g, 56%) as blue solid. mp 172−173 °C. ^{1}H NMR (400 MHz, $CDCl_3$) δ 7.46−7.28 (m, 4H), 7.17 (t, J = 7.4 Hz, 1H), 7.01 (d, J = 7.9 Hz, 1H), 6.82 (dd, J = 13.3, 8.4 Hz, 1H), 6.06−5.83 (m, 2H), 4.01 (d, J = 7.1 Hz, 2H), 3.91 (s, 2H), 1.81 (s, 2H), 1.78 (d, J = 5.6 Hz, 12H), 1.72 (s, 2H), 1.45−1.28 (m, 12H), 0.89 (t, J = 6.5 Hz, 6H). ^{13}C NMR (101 MHz, $CDCl_3$) δ 181.1, 171.2, 168.6, 142.5, 130.8, 130.7, 128.0, 125.9, 125.8, 124.2, 122.5, 116.7, 116.2, 110.5, 109.8, 87.1, 86.9, 49.7, 49.2, 44.0, 31.6, 31.6, 29.8, 27.3, 27.2, 27.1, 27.0, 26.9, 26.8, 22.66, 22.65, 22.6, 14.1. HRMS (ESI) m/z $[M + H]^+$ Calcd for $C_{38}H_{48}BrN_2O_2$ 643.2899, found 643.2885.

*4,8-Dimethoxybenzo[1,2-b:4,5-b′]dithiophene-2-carbaldehyde (**9a**).* In a two necked round-bottom flask fitted with reflux condenser, **8a** (1.2 g, 5.20 mmol) was taken. It was dissolved in 20 mL of 1,2-dichloroethane and *N*,*N*-dimethylformamide (8 mL, 104 mmol) was added to the mixture. The flask was cooled to 0 °C and $POCl_3$ (9.5 mL, 104 mmol) was added to it dropwise and refluxed for 24 h. After completion of reaction the reaction mixture was poured in ice cold solution of ammonium chloride and extracted by dichloromethane. The organic layer was dried over sodium sulfate and solvents were removed under reduced pressure. The crude product was purified by column chromatography over silica gel with ethyl acetate/pet ether as eluent to afford **8a** (1.2 g, 80%) as light yellow solid. mp 140−143 °C. ^{1}H NMR (200 MHz, $CDCl_3$) δ 10.10 (s, 1H), 8.23 (s, 1H), 7.52 (s, 2H), 4.22 (s, 3H), 4.13 (s, 3H). ^{13}C NMR (101 MHz, $CDCl_3$) δ 184.6, 148.0, 145.4, 143.0, 135.1, 131.6, 131.3, 130.1, 129.6, 128.9, 120.4, 61.5, 61.2. HRMS (ESI) m/z $[M + H]^+$ Calcd for $C_{13}H_{11}O_3S_2$ 279.0150, found 279.0140.

*4,8-Bis((2-ethylhexyl)oxy)benzo[1,2-b:4,5-b′]dithiophene-2-carbaldehyde (**9b**).* In a two necked round-bottom flask fitted with reflux condenser, **8b** (2.8 g, 6.27 mmol) was taken. It was dissolved in 20 mL of 1,2-dichloroethane and *N*,*N*-dimethylformamide (9.76 mL, 125.4 mmol) was added to the mixture. The flask was cooled to 0 °C and $POCl_3$ (11.7 mL, 125.361 mmol) was added to it dropwise and refluxed for 48 h. After completion of reaction the reaction mixture was poured in ice cold solution of ammonium chloride and extracted by dichloromethane. The organic layer was dried over sodium sulfate and solvents were removed under reduced pressure. The crude product was purified by column chromatography over silica gel with ethyl acetate/pet ether as eluent to afford **8a** ((2 g, 67%) as yellow viscous oil. ^{1}H NMR (400 MHz, $CDCl_3$) δ 10.10 (s, 1H), 8.17 (s, 1H), 7.49 (s, 2H), 4.27 (d, J = 5.4 Hz, 2H), 4.18−4.15 (m, 2H), 1.82 (dd, J = 12.0, 6.0 Hz, 2H), 1.75−1.65 (m, 2H), 1.62−1.56 (m, 4H), 1.54−1.47 (m, 2H), 1.41−1.35 (m, 8H), 1.05−0.99 (m, 6H), 0.97−0.90 (m, 6H). ^{13}C NMR (101 MHz, $CDCl_3$) δ 184.7, 147.4, 144.7, 142.7, 135.3, 131.9, 131.5, 130.3, 129.9, 128.6, 120.6, 76.7, 76.4, 40.8, 30.5, 29.3, 24.0, 23.2, 14.3, 11.4. HRMS (ESI) m/z $[M + H]^+$ Calcd for $C_{27}H_{39}O_3S_2$ 475.2341, found 475.2333.

General Synthetic Procedure for Direct Arylation of Squaraine and BDT. In a Schlenk tube corresponding bromo-squaraine (7) and BDT aldehydes (**9a** and **9b**) were taken. The Shclenk tube is evacuated and refilled with nitrogen three times. $Pd(OAc)_2$ (5 mol %), PCy_3(10 mol %), PivOH (30 mol %) and K_2CO_3 (2.5 equiv) were added to it followed by 4 mL of anhydrous toluene. The mixture was stirred at 110 °C for 24 h. After completion of the reaction, the mixture was poured into water and extracted with dichloromethane. The organic layer was then washed with brine, dried over sodium sulfate and concentrated under vacuum. Crude product was purified by column chromatography to give of pure compounds.

*(Z)-4-((5-(6-Formyl-4,8-dimethoxybenzo[1,2-b:4,5-b′]dithiophen-2-yl)-1-hexyl-3,3-dimethyl-3H-indol-1-ium-2-yl)methylene)-2-(((Z)-1-hexyl-3,3-dimethylindolin-2-ylidene)methyl)-3-oxocyclobut-1-en-1-olate (**10a**).* From bromo-squaraine 7 (0.250 g, 0.388 mmol) and aldehyde 9a (0.432 g, 1.55 mmol), the compound 10a (0.2 g, 61%) was obtained as green solid. mp 251−253 °C. ^{1}H NMR (500 MHz, $CDCl_3$) δ 10.10 (s, 1H), 8.22 (s, 1H), 7.71 (d, J = 1.7 Hz, 1H), 7.69 (s, 1H), 7.69 (s, 1H), 7.39 (d, J = 7.3 Hz, 1H), 7.33 (td, J = 7.8, 0.9 Hz, 1H), 7.18 (t, J = 7.3 Hz, 1H), 7.02 (dd, J = 10.3, 8.5 Hz, 2H), 6.03 (s, 1H), 6.00 (s, 1H), 4.26 (s, 3H), 4.18 (s, 3H), 4.06−4.01 (m, 2H), 4.00−3.94 (m, 2H), 1.88 (s, 6H), 1.81 (s, 6H), 1.50−1.40 (m, 6H), 1.37−1.31 (m, 10H), 0.92−0.88 (m, 6H).^{13}C NMR (126 MHz, $CDCl_3$) δ 184.5, 181.3, 178.4, 171.4, 168.5, 147.6, 146.5, 145.0, 142.6, 142.4, 136.4, 131.8, 131.6, 130.2, 129.0, 128.5, 128.0, 126.9, 124.3, 122.5, 120.6, 114.8, 109.9, 109.5, 87.2, 61.4, 61.2, 49.8, 49.1, 44.1, 43.9, 31.63, 31.61, 29.8, 27.5, 27.33, 27.25, 27.13, 27.05, 26.9, 22.7, 14.1. HRMS (ESI) m/z $[M + H]^+$ Calcd for $C_{51}H_{57}N_2O_5S_2$ 841.3709, found 841.3701.

*(Z)-4-((5-(4,8-Bis((2-ethylhexyl)oxy)-6-formylbenzo[1,2-b:4,5-b′]-dithiophen-2-yl)-1-hexyl-3,3-dimethyl-3H-indol-1-ium-2-yl)-methylene)-2-(((Z)-1-hexyl-3,3-dimethylindolin-2-ylidene)methyl)-3-oxocyclobut-1-en-1-olate (**10b**).* From bromo-squaraine 7 (0.200 g, 0.310 mmol) and aldehyde **9b** (0.589 g, 1.24 mmol), 0.150 g of compound **10b** (0.15 g, 46%) was obtained as green sticky gum. ^{1}H NMR (400 MHz, $CDCl_3$) δ 10.10 (s, 1H), 8.17 (s, 1H), 7.69 (d, J = 8.3 Hz, 1H), 7.66 (s, 1H), 7.63 (s, 1H), 7.39 (d, J = 7.3 Hz, 1H), 7.33 (t, J = 7.6 Hz, 1H), 7.18 (t, J = 7.4 Hz, 1H), 7.02 (dd, J = 7.5, 5.4 Hz, 2H), 6.03 (s, 1H), 6.00 (s, 1H), 4.32 (d, J = 5.4 Hz, 2H), 4.21 (d, J = 5.2 Hz, 2H), 4.06−3.95 (m, 4H), 1.87 (s, 6H), 1.81 (s, 6H), 1.73−1.53 (m, 10H), 1.47−1.39 (m, 14H), 1.36−1.25 (m, 10H), 1.05 (t, J = 7.3 Hz, 6H), 0.97−0.89 (m, 12H). ^{13}C NMR (101 MHz, $CDCl_3$) δ 184.6, 181.3, 178.5, 171.3, 168.5, 147.1, 146.1, 144.4, 142.4, 136.6, 132.0, 131.9, 130.3, 129.2, 128.7, 128.0, 126.8, 124.329, 122.5, 120.6, 115.0, 109.9, 87.2, 76.6, 76.3, 49.8, 49.1, 44.1, 40.8, 40.8, 31.6, 30.6, 30.5, 29.3, 27.4, 27.3, 27.13, 27.07, 26.9, 24.0, 23.3, 22.7, 14.3, 14.1, 11.5. HRMS (ESI) m/z $[M + H]^+$ Calcd for $C_{65}H_{85}N_2O_5S_2$ 1037.5900, found 1037.5876.

DOI: 10.1021/acs.joc.6b02670
J. Org. Chem. 2017, 82, 1920−1930

General Procedure for Knoevenagel Condenstation of Aldehyde to Cyanoacetic Acid. Corresponding aldehydes (**10a** and **10b**) were dissolved in 5 mL of chloroform and 5 mL of acetonitrile. To this 5 equiv cyanoacetic acid was added followed by 40 μL of piperidine. The resultant solution was stirred at 80 °C for 16 h. Solvents were removed under rotavap after completion of reaction and dissolved in 50 mL of dichloromethane. The organic layer was washed with water followed by brine and dried over sodium sulfate. The solvents were removed under reduced pressure and purified by column chromatography by silica gel using MeOH/$CHCl_3$ as an eluent.

4-((5-(6-(2-Carboxy-2-cyanovinyl)-4,8-dimethoxybenzo[1,2-b:4,5-b′]dithiophen-2-yl)-1-hexyl-3,3-dimethyl-3H-indol-1-ium-2-yl)methylene)-2-((1-hexyl-3,3-dimethylindolin-2-ylidene)methyl)-3-oxocyclobut-1-en-1-olate (RSQ-1). From **10a** (0.15 g, 0.178 mmol), pure compound RSQ-1 (0.1 g, 62%) was obtained as dark green solid. mp 281−283 °C.. ^{1}H NMR (400 MHz, DMSO-d_6 + $CDCl_3$) δ 8.30 (s, 1H), 7.95 (s, 1H), 7.67 (d, *J* = 9.7 Hz, 2H), 7.62 (d, *J* = 8.1 Hz, 1H), 7.33 (d, *J* = 7.3 Hz, 1H), 7.27 (t, *J* = 7.6 Hz, 1H), 7.11 (t, *J* = 7.4 Hz, 1H), 7.05 (t, *J* = 8.4 Hz, 2H), 5.88 (s, 1H), 5.84 (s, 1H), 4.12 (s, 3H), 4.07 (s, 3H), 4.04−3.89 (m, 4H), 1.75 (s, 6H), 1.69 (s, 6H), 1.40−1.16 (m, 16H), 0.81 (t, *J* = 6.5 Hz, 6H). ^{13}C NMR (101 MHz, DMSO-d_6 + $CDCl_3$) δ 181.3, 180.1, 170.2, 167.7, 145.6, 145.1, 143.8, 143.1, 142.8, 142.3, 141.7, 141.5, 135.7, 134.4, 130.7, 129.2, 128.9, 128.4, 127.9, 127.5, 126.3, 123.8, 121.8, 119.7, 117.6, 114.3, 109.6, 109.4, 86.3, 63.0, 60.7, 60.6, 48.9, 48.3, 43.1, 30.9, 29.0, 26.7, 26.5, 26.3, 26.0, 21.9, 13.5. HRMS (ESI) *m*/*z* [M]$^+$ Calcd for $C_{54}H_{57}N_3O_6S_2$ 907.3689, found 907.3683.

4-((5-(6-(2-Carboxy-2-cyanovinyl)-4,8-bis((2-ethylhexyl)oxy)benzo[1,2-b:4,5-b′]dithiophen-2-yl)-1-hexyl-3,3-dimethyl-3H-indol-1-ium-2-yl)methylene)-2-((1-hexyl-3,3-dimethylindolin-2-ylidene)-methyl)-3-oxocyclobut-1-en-1-olate (RSQ-2). From **10b** (0.1 g, 0.097 mmol), compound RSQ-2 (0.065, 61%) was obtained as dark green solid. mp 242−243 °C. ^{1}H NMR (400 MHz, DMSO-d_6 + $CDCl_3$) δ 8.38 (s, 1H), 8.08 (s, 1H), 7.63 (d, *J* = 7.0 Hz, 2H), 7.58 (s, 1H), 7.35 (d, *J* = 7.3 Hz, 1H), 7.28 (t, *J* = 7.6 Hz, 1H), 7.11 (dd, *J* = 14.5, 7.6 Hz, 3H), 5.88 (s, 1H), 5.84 (s, 1H), 4.21 (d, *J* = 4.9 Hz, 2H), 4.13 (d, *J* = 4.2 Hz, 3H), 4.05−3.93 (m, 4H), 1.77 (s, 6H), 1.70 (s, 6H), 1.65−1.43 (m, 10H), 1.42−1.32 (m, 14H), 1.30−1.16 (m, 10H), 0.98 (dd, *J* = 16.7, 7.6 Hz, 6H), 0.91−0.87 (m, 6H), 0.83 (t, *J* = 6.2 Hz, 6H). ^{13}C NMR (101 MHz, $CDCl_3$) δ 181.1, 180.2, 177.4, 170.2, 167.5, 145.4, 145.3, 143.0, 142.9, 142.1, 141.7, 141.4, 135.1, 134.8, 131.3, 128.9, 128.3, 128.1, 127.5, 126.3, 123.7, 121.7, 119.5, 116.0, 115.9, 114.3, 109.7, 109.6, 86.5, 86.3, 78.2, 75.9, 75.4, 49.5, 48.9, 48.2, 43.2, 30.8, 29.9, 29.7, 28.6, 28.5, 26.6, 26.5, 26.3, 26.0, 23.2, 22.49, 22.46, 21.9, 13.7, 13.5, 10.9. HRMS (ESI) *m*/*z* [M + H]$^+$ Calcd for $C_{68}H_{86}N_3O_6S_2$ 1104.5958, found 1104.5946.

Solar Cells Fabrication and Characterization. FTO (F-doped SnO_2 glass; 6−8 Ω /sq; Pilkington TEC 7) was cleaned by diluted mucasol solution in water, deionized water, and ethanol, successively. To grow a TiO_2 blocking layer, the substrate was immersed in freshly prepared 50 mM aqueous $TiCl_4$ solution at 70 °C for 30 min, and washed with deionized water before drying at 125 °C for 10 min. A paste of TiO_2 nanocrystal (<20 nm, Ti-Nanoxide T/SP, Solaronix) was deposited by the doctor-blade technique on TiO_2 buffer layer coated FTO substrate for transparent layer of TiO_2, kept in air for 5 min and then annealed at 125 °C in air for 15 min. The films were about 6−8 μm thick. The annealed films were coated with scattering layer TiO_2 paste (WER2-O, Dyesol) and annealed at 125 °C in air for 15 min. The annealed films were sintered at 325 °C for 5 min, 375 °C for 5 min, 450 °C for 15 min and 500 °C for 15 min with heating rate of 5 °C per min in air. After reaching the furnace temperature at 50 °C, sintered films were immersed in freshly prepared 50 mM aqueous $TiCl_4$ solution at 70 °C for 30 min. After sintering the $TiCl_4$-treated TiO_2 films at 500 °C for 30 min, they were immediately immersed in 0.1 mM RSQ dye solution in dichloromethane for 5 h, washed and dried at 80 °C. In case of CDCA added experiments, different ratio of CDCA added to 0.1 mM dye solution and photoanode dipped for 5 h. Sandwich type cell configuration was completed using platinum as cathode, 0.5 M DMII, 0.1 M LiI, 0.1 M I_2 and 10 mM TBP in CH_3CN was used as electrolyte and 25 μm spacer. *I*−*V* characteristics of the cells were measured using Keithley digital source meter (2420, Keithley, USA) controlled by a computer and standard AM 1.5 solar simulator (PET, CT200AAA, USA). To measure the photocurrent and voltage, an external bias of AM 1.5G light was applied using a xenon lamp (450 W, USHIO INC, Philippines) and recorded. The action spectra of monochromatic incident photon-to-current conversion efficiency (IPCE) for the solar cell were performed by using a commercial setup. Electrochemical impedance spectra (EIS) were obtained by the Biologic potentiostat, equipped with an FRA2 module, with applied potential of −0.45 V in the dark. The frequency range explored was 1 Hz to 1 MHz with an ac perturbation of 10 mV. The impedance spectra were analyzed using an equivalent circuit model of R1+R2/C2+R3/C3. The loading amount of the dyes was assessed by UV−vis spectrophotometry as follows: Photoanodes were sensitized in same dye solutions which were used for photovoltaic characterization. The photoanodes were taken out and dyes were desorbed by dipping in 2 M solution of HCl in EtOH. The resultant dye solution was used to evaluate the dye concentration by UV−vis study, which allows the determination of the amount of dye adsorbed in terms of number of moles per unit area of TiO_2 film.

Light harvesting efficiency was obtained by

$$\mathrm{LHE} = 1 - 10^{-\varepsilon\Gamma} = 1 - 10^{-A} \quad (1)$$

where ε is the molar extinction coefficient of the dye sensitized on TiO_2 film, Γ is the dye molar concentration per projected surface area of the film, and *A* is the absorbance of the dye-sensitized film (equal to the product of ε and Γ).[57]

■ ASSOCIATED CONTENT

Supporting Information

The Supporting Information is available free of charge on the ACS Publications website at DOI: 10.1021/acs.joc.6b02670.

^{1}H and ^{13}C NMR spectra, HRMS spectra, Computational studies, Cartesian coordinates, Dye desorption study, Absorption and emission curves, Quantum yield calculation and Differential Pulse Voltammogram (PDF)

■ AUTHOR INFORMATION

Corresponding Author

*Tel: +91-020-25903050. E-mail: j.nithyanandhan@ncl.res.in.

ORCID

Jayaraj Nithyanandhan: 0000-0002-3429-4989

Notes

The authors declare no competing financial interest.

■ ACKNOWLEDGMENTS

The financial support by CSIR-Network Project NWP0054 (CSIR-TAPSUN) is greatly acknowledged. R. B. and A. K. S. thank CSIR for fellowship. J. N. thanks Dr. Kothandam Krishnamoorthy, Polymer Science Engineering Division, CSIR-National Chemical Laboratory, Pune, India for his support, help with device fabrication and characterization. The authors also thank Ms. Neeta Karjule for help with mass spectrometric experiments.

■ REFERENCES

(1) Grätzel, M. *J. Photochem. Photobiol., C* **2003**, *4*, 145−153.

(2) Hagfeldt, A.; Boschloo, G.; Sun, L.; Kloo, L.; Pettersson, H. *Chem. Rev.* **2010**, *110*, 6595−6663.

(3) Chen, C.-Y.; Wang, M.; Li, J.-Y.; Pootrakulchote, N.; Alibabaei, L.; Ngoc-le, C.; Decoppet, J.-D.; Tsai, J.-H.; Grätzel, C.; Wu, C.-G.; Zakeeruddin, S. M.; Grätzel, M. *ACS Nano* **2009**, *3*, 3103−3109.

(4) Mathew, S.; Yella, A.; Gao, P.; Humphry-Baker, R.; Curchod, B. F. E.; Ashari-Astani, N.; Tavernelli, I.; Rothlisberger, U.; Nazeeruddin, M. K.; Grätzel, M. *Nat. Chem.* **2014**, *6*, 242−247.

DOI: 10.1021/acs.joc.6b02670
J. Org. Chem. 2017, 82, 1920−1930

(5) Mishra, A.; Fischer, M. K. R.; Bäuerle, P. *Angew. Chem., Int. Ed.* **2009**, *48*, 2474−2499.
(6) Zhou, N.; Prabakaran, K.; Lee, B.; Chang, S. H.; Harutyunyan, B.; Guo, P.; Butler, M. R.; Timalsina, A.; Bedzyk, M. J.; Ratner, M. A.; Vegiraju, S.; Yau, S.; Wu, C.-G.; Chang, R. P. H.; Facchetti, A.; Chen, M.-C.; Marks, T. J. *J. Am. Chem. Soc.* **2015**, *137*, 4414−4423.
(7) Yao, Z.; Zhang, M.; Wu, H.; Yang, L.; Li, R.; Wang, P. *J. Am. Chem. Soc.* **2015**, *137*, 3799−3802.
(8) Li, L.-L.; Diau, E. W.-G. *Chem. Soc. Rev.* **2012**, *42*, 291−304.
(9) Yella, A.; Lee, H.-W.; Tsao, H. N.; Yi, C.; Chandiran, A. K.; Nazeeruddin, M. K.; Diau, E. W.-G.; Yeh, C.-Y.; Zakeeruddin, S. M.; Grätzel, M. *Science* **2011**, *334*, 629−634.
(10) Urbani, M.; Grätzel, M.; Nazeeruddin, M. K.; Torres, T. *Chem. Rev.* **2014**, *114*, 12330−12396.
(11) Wang, C.-L.; Zhang, M.; Hsiao, Y.-H.; Tseng, C.-K.; Liu, C.-L.; Xu, M.; Wang, P.; Lin, C.-Y. *Energy Environ. Sci.* **2016**, *9*, 200−206.
(12) Martín-Gomis, L.; Fernández-Lázaro, F.; Sastre-Santos, Á. *J. Mater. Chem. A* **2014**, *2*, 15672−15682.
(13) Ragoussi, M.-E.; Ince, M.; Torres, T. *Eur. J. Org. Chem.* **2013**, *2013*, 6475−6489.
(14) Saccone, D.; Galliano, S.; Barbero, N.; Quagliotto, P.; Viscardi, G.; Barolo, C. *Eur. J. Org. Chem.* **2016**, *2016*, 2244−2259.
(15) Mishra, A.; Behera, R. K.; Behera, P. K.; Mishra, B. K.; Behera, G. B. *Chem. Rev.* **2000**, *100*, 1973−2012.
(16) Beverina, L.; Salice, P. *Eur. J. Org. Chem.* **2010**, *2010*, 1207−1225.
(17) Qin, C.; Wong, W.-Y.; Han, L. *Chem. - Asian J.* **2013**, *8*, 1706−1719.
(18) Escobedo, J. O.; Rusin, O.; Lim, S.; Strongin, R. M. *Curr. Opin. Chem. Biol.* **2010**, *14*, 64−70.
(19) Luo, S.; Zhang, E.; Su, Y.; Cheng, T.; Shi, C. *Biomaterials* **2011**, *32*, 7127−7138.
(20) Ajayaghosh, A. *Acc. Chem. Res.* **2005**, *38*, 449−459.
(21) Ramaiah, D.; Eckert, I.; Arun, K. T.; Weidenfeller, L.; Epe, B. *Photochem. Photobiol.* **2002**, *76*, 672−677.
(22) Ramaiah, D.; Eckert, I.; Arun, K. T.; Weidenfeller, L.; Epe, B. *Photochem. Photobiol.* **2004**, *79*, 99−104.
(23) Shi, Y.; Hill, R. B. M.; Yum, J.-H.; Dualeh, A.; Barlow, S.; Grätzel, M.; Marder, S. R.; Nazeeruddin, M. K. *Angew. Chem., Int. Ed.* **2011**, *50*, 6619−6621.
(24) Delcamp, J. H.; Shi, Y.; Yum, J.-H.; Sajoto, T.; Dell'Orto, E.; Barlow, S.; Nazeeruddin, M. K.; Marder, S. R.; Grätzel, M. *Chem. - Eur. J.* **2013**, *19*, 1819−1827.
(25) Alex, S.; Santhosh, U.; Das, S. *J. Photochem. Photobiol., A* **2005**, *172*, 63−71.
(26) Otsuka, A.; Funabiki, K.; Sugiyama, N.; Yoshida, T.; Minoura, H.; Matsui, M. *Chem. Lett.* **2006**, *35*, 666−667.
(27) Kuster, S.; Sauvage, F.; Nazeeruddin, M. K.; Grätzel, M.; Nüesch, F. A.; Geiger, T. *Dyes Pigm.* **2010**, *87*, 30−38.
(28) Pandey, S. S.; Inoue, T.; Fujikawa, N.; Yamaguchi, Y.; Hayase, S. *Thin Solid Films* **2010**, *519*, 1066−1071.
(29) Li, C.; Wang, W.; Wang, X.; Zhang, B.; Cao, Y. *Chem. Lett.* **2005**, *34*, 554−555.
(30) Mulhern, K. R.; Detty, M. R.; Watson, D. F. *J. Photochem. Photobiol., A* **2013**, *264*, 18−25.
(31) Mann, J. R.; Gannon, M. K.; Fitzgibbons, T. C.; Detty, M. R.; Watson, D. F. *J. Phys. Chem. C* **2008**, *112*, 13057−13061.
(32) de Miguel, G.; Ziółek, M.; Zitnan, M.; Organero, J. A.; Pandey, S. S.; Hayase, S.; Douhal, A. *J. Phys. Chem. C* **2012**, *116*, 9379−9389.
(33) Yum, J.-H.; Walter, P.; Huber, S.; Rentsch, D.; Geiger, T.; Nüesch, F.; De Angelis, F.; Grätzel, M.; Nazeeruddin, M. K. *J. Am. Chem. Soc.* **2007**, *129*, 10320−10321.
(34) Geiger, T.; Kuster, S.; Yum, J.-H.; Moon, S.-J.; Nazeeruddin, M. K.; Grätzel, M.; Nüesch, F. *Adv. Funct. Mater.* **2009**, *19*, 2720−2727.
(35) Jradi, F. M.; Kang, X.; O'Neil, D.; Pajares, G.; Getmanenko, Y. A.; Szymanski, P.; Parker, T. C.; El-Sayed, M. A.; Marder, S. R. *Chem. Mater.* **2015**, *27*, 2480−2487.
(36) Alagumalai, A.; M. K., M. F.; Vellimalai, P.; Sil, M. C.; Nithyanandhan, J. *ACS Appl. Mater. Interfaces* **2016**, *8*, 35353−35367.
(37) Yao, H.; Ye, L.; Zhang, H.; Li, S.; Zhang, S.; Hou, J. *Chem. Rev.* **2016**, *116*, 7397−7457.
(38) Pai, R. K.; Ahipa, T. N.; Hemavathi, B. *RSC Adv.* **2016**, *6*, 23760−23774.
(39) Hao, X.; Liang, M.; Cheng, X.; Pian, X.; Sun, Z.; Xue, S. *Org. Lett.* **2011**, *13*, 5424−5427.
(40) Longhi, E.; Bossi, A.; Di Carlo, G.; Maiorana, S.; De Angelis, F.; Salvatori, P.; Petrozza, A.; Binda, M.; Roiati, V.; Mussini, P. R.; Baldoli, C.; Licandro, E. *Eur. J. Org. Chem.* **2013**, *2013*, 84−94.
(41) Chen, Y.-F.; Liu, J.-M.; Huang, J.-F.; Tan, L.-L.; Shen, Y.; Xiao, L.-M.; Kuang, D.-B.; Su, C.-Y. *J. Mater. Chem. A* **2015**, *3*, 8083−8090.
(42) Ackermann, L.; Vicente, R.; Kapdi, A. *Angew. Chem., Int. Ed.* **2009**, *48*, 9792−9826.
(43) Alberico, D.; Scott, M. E.; Lautens, M. *Chem. Rev.* **2007**, *107*, 174−238.
(44) Battace, A.; Lemhadri, M.; Zair, T.; Doucet, H.; Santelli, M. *Adv. Synth. Catal.* **2007**, *349*, 2507−2516.
(45) Völker, S. F.; Renz, M.; Kaupp, M.; Lambert, C. *Chem. - Eur. J.* **2011**, *17*, 14147−14163.
(46) Mamada, M.; Kumaki, D.; Nishida, J.; Tokito, S.; Yamashita, Y. *ACS Appl. Mater. Interfaces* **2010**, *2*, 1303−1307.
(47) Mei, C.-Y.; Liang, L.; Zhao, F.-G.; Wang, J.-T.; Yu, L.-F.; Li, Y.-X.; Li, W.-S. *Macromolecules* **2013**, *46*, 7920−7931.
(48) Urbani, M.; Medel, M.; Kumar, S. A.; Ince, M.; Bhaskarwar, A. N.; González-Rodríguez, D.; Grätzel, M.; Nazeeruddin, M. K.; Torres, T. *Chem. - Eur. J.* **2015**, *21* (45), 16252−16265.
(49) Schipper, D. J.; Fagnou, K. *Chem. Mater.* **2011**, *23*, 1594−1600.
(50) Unger, E. L.; Morandeira, A.; Persson, M.; Zietz, B.; Ripaud, E.; Leriche, P.; Roncali, J.; Hagfeldt, A.; Boschloo, G. *Phys. Chem. Chem. Phys.* **2011**, *13*, 20172−20177.
(51) Alex, S.; Santhosh, U.; Das, S. *J. Photochem. Photobiol., A* **2005**, *172*, 63−71.
(52) Park, J.; Barolo, C.; Sauvage, F.; Barbero, N.; Benzi, C.; Quagliotto, P.; Coluccia, S.; Censo, D. D.; Grätzel, M.; Nazeeruddin, M. K.; Viscardi, G. *Chem. Commun.* **2012**, *48*, 2782−2784.
(53) Kalyanasundaram, K.; Grätzel, M. *Coord. Chem. Rev.* **1998**, *177*, 347−414.
(54) Frisch, M. J. et al. *Gaussian 09*, Revision A.02; Gaussian, Inc.: Wallingford, CT, 2009. (Complete reference is provided in the Supporting Information).
(55) Wang, Q.; Moser, J.-E.; Grätzel, M. *J. Phys. Chem. B* **2005**, *109*, 14945−14953.
(56) Longo, C.; Nogueira, A. F.; De Paoli, M.-A.; Cachet, H. *J. Phys. Chem. B* **2002**, *106*, 5925−5930.
(57) Yum, J.-H.; Baranoff, E.; Kessler, F.; Moehl, T.; Ahmad, S.; Bessho, T.; Marchioro, A.; Ghadiri, E.; Moser, J.-E.; Yi, C.; Nazeeruddin, M. K.; Grätzel, M. *Nat. Commun.* **2012**, *3*, 631.

DOI: 10.1021/acs.joc.6b02670
J. Org. Chem. 2017, 82, 1920−1930